

Polyoxometalates | Hot Paper |

Covalent Immobilization of Polyoxotungstate on Alumina and Its Catalytic Generation of Sulfoxides

Lanlan Hong,^[a] Pyaesone Win,^[a] Xuan Zhang,^[a] Wei Chen,^{*,[a]} Haralampos N. Miras,^[b] and Yu-Fei Song^{*,[a]}

Abstract: The structural and chemical stabilities of immobilized polyoxometalate (POM)-containing catalysts are crucial factors for their industrial application. An alumina supported POM catalyst is prepared by using a facile condensation reaction between the trilacunary POM $\text{Na}_{12}[\alpha\text{-P}_2\text{W}_{15}\text{O}_{56}]\cdot 24\text{H}_2\text{O}$ (P_2W_{15}) and the hydroxy groups on the surface of $\gamma\text{-Al}_2\text{O}_3$ spheres under acidic conditions. The heterogeneous catalyst $\text{P}_2\text{W}_{15}\text{-Al}_2\text{O}_3$ is characterized by a wide variety of techniques

and shows excellent stability and highly efficient reactivity and selectivity for the oxygenation of thioethers to sulfoxides, which are a very useful intermediate in organic synthesis and the industrial preparation of drugs. Furthermore, $\text{P}_2\text{W}_{15}\text{-Al}_2\text{O}_3$ can be recycled and reused at least ten times without any observable loss of its catalytic efficiency, mainly due to the covalent immobilization and high dispersion of P_2W_{15} on the $\gamma\text{-Al}_2\text{O}_3$ surface.

Introduction

Polyoxometalates (POMs) are a class of discrete anionic metal oxides, often incorporating V, Mo, W, or Nb, among other metals,^[1] in their highest oxidation states. They exhibit unique structural archetypes, as well as a wide range of sizes, unique physical properties,^[2] and applications^[3] in areas as diverse as catalysis, medicine, electrochemistry, photochromism, and magnetism.^[4] Additionally, their solution processability, due to their high solubility,^[1] low lattice energies,^[2] and generally weak interactions between the POM clusters and their associated counterions (e.g., NH_4^+ , K^+ , Na^+), render them ideal candidates and useful components for the design of functional materials such as catalysts. More specifically, studies on POM-based catalysis are mainly focused on the design of simplified routes for the preparation of heterogeneous systems due to catalyst recoverability, reusability and excellent chemical, structural and thermal stability.^[3]

Immobilization and solidification of POM species on various substrates are two widely applied approaches for the generation of multifunctional POM-based heterogeneous catalysts.^[3,4] Although great efforts have been made for the efficient immobilization of POMs on supports such as SiO_2 ,^[5] Al_2O_3 ,^[6] ZrO_2 ,^[7]

zeolites,^[8] and activated carbons,^[9] the produced composite materials have tended to suffer from various issues that need to be taken into consideration. For example, heterogeneous catalysts based on the electrostatic interactions developed between the POM species and the supports suffer from stability issues owing to POM leaching,^[10-12] whereas the production of heterogeneous catalysts under high temperature regimes (e.g., calcination) usually leads to structural rearrangements and compromises the POMs' structural integrity, which greatly limits opportunities to exploit the wide range of functionalities directly correlated to the POMs' structural features.^[6,13,14] Therefore, utilization of robust support surfaces that preserve the POM's structural integrity for the development of heterogeneous catalysts for a wide range of processes is highly desirable.

The spherical $\gamma\text{-Al}_2\text{O}_3$ exhibits remarkable physical properties such as mechanical stability, well-defined pore structure and high specific surface areas. For these reasons, it is widely employed in the chemical and petrochemical industries.^[15-22] Herein we report the preparation of a composite material by covalent immobilization of $\text{Na}_{12}[\alpha\text{-P}_2\text{W}_{15}\text{O}_{56}]\cdot 24\text{H}_2\text{O}$ (P_2W_{15}) POM clusters onto spherical $\gamma\text{-Al}_2\text{O}_3$ particles (Scheme 1) and we discuss its catalytic efficacy for the selective oxygenation of thioethers.

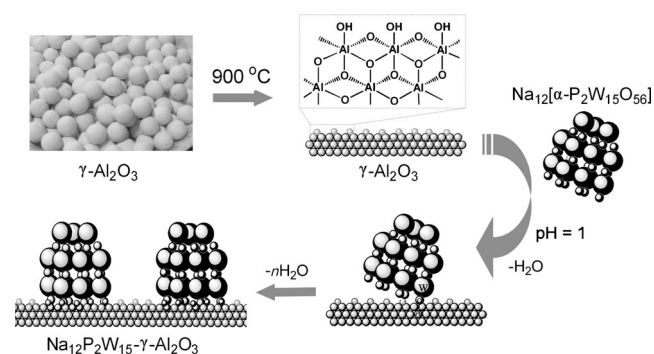
Results and Discussion

The $\text{P}_2\text{W}_{15}\text{-Al}_2\text{O}_3$ composite material was synthesized by immobilization of $\text{Na}_{12}[\alpha\text{-P}_2\text{W}_{15}\text{O}_{56}]\cdot 24\text{H}_2\text{O}$ clusters onto the surface of the spherical $\gamma\text{-Al}_2\text{O}_3$ particles under acidic conditions.^[23,24] In an effort to optimize the immobilization conditions, we immobilized the POM clusters under conditions ranging from pH 6 to pH 1 (Figure 1). The resultant solids were separated from the reaction mixture by filtration and washed with 0.3 M

[a] L. Hong, P. Win, X. Zhang, Dr. W. Chen, Prof. Y.-F. Song
State Key Laboratory of Chemical Resource Engineering
Beijing University of Chemical Technology, Beijing 100029 (P. R. China)
E-mail: chenw@mail.buct.edu.cn
songyufeihotmail.com
songyf@mail.buct.edu.cn

[b] Dr. H. N. Miras
WestCHEM, School of Chemistry
University of Glasgow, Glasgow, G12 8QQ (UK)

Supporting information for this article is available on the WWW under <http://dx.doi.org/10.1002/chem.201601864>.



Scheme 1. Synthesis of $P_2W_{15}-Al_2O_3$.

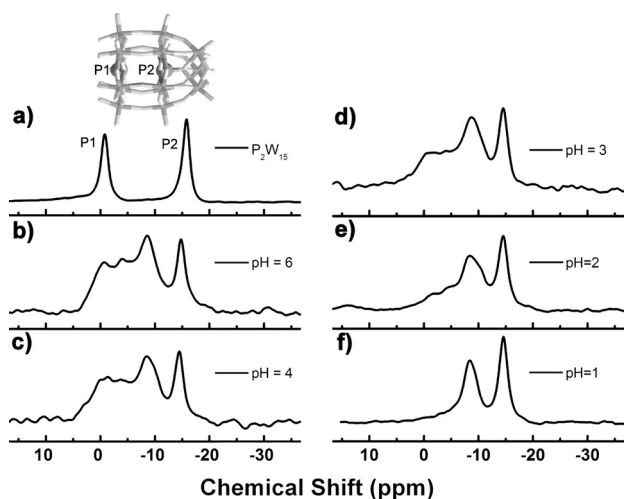
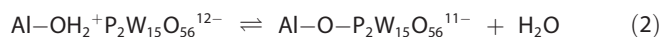
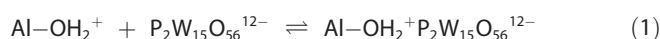


Figure 1. Solid-state ^{31}P NMR spectra: a) $Na_{12}[\alpha-P_2W_{15}O_{56}] \cdot 24H_2O$; b-f) $P_2W_{15}-Al_2O_3$ composite material prepared under different pH environments.

LiCl solution to remove the physically adsorbed $\{P_2W_{15}\}$ clusters.^[25]

Figure 1a shows part of the solid-state ^{31}P NMR spectrum of $Na_{12}[\alpha-P_2W_{15}O_{56}] \cdot 24H_2O$, where the signals at $\delta = -0.79$ and -15.77 ppm can be assigned to the nonequivalent phosphorus atoms P1 and P2, respectively.^[26] Upon decrease of the pH value from 6 to 1, the left shoulder peak centered at -0.79 ppm decreases and splits into several peaks in the range of -0.79 to -8.41 ppm, which is a potential indication of partial decomposition at specific pH values of the cluster prior to immobilization on the alumina surface. The signal at $\delta = -15.77$ ppm, shifts gradually to -14.58 ppm, as a result of the reaction between the $\{P_2W_{15}\}$ anions and the $\gamma-Al_2O_3$ surface. According to the solid state ^{31}P NMR spectra, the most effective immobilization of the lacunary Dawson anions onto the alumina support takes place at pH 1. This is in agreement with the Mulcahy's report,^[23] where the positive net surface charge acquired at pH values below the isoelectric point (IEP) of the support, attracts and stabilizes the anionic species from the bulk solution. However, a simple electrostatic model cannot account for the adsorption of these anions. It is suggested that this is a two-step process whereby the electrostatic ion pairing occurs first as soon as the pH value is below 8.6, the IEP of $\gamma-Al_2O_3$ (see the Supporting Information, Figure S1), followed by

a condensation reaction between the $\{P_2W_{15}\}$ anions and the $\gamma-Al_2O_3$ surface according to the Equations (1) and (2):



The $W=O$ and $W-O$ stretching and bending vibrations of the P_2W_{15} generally occur below 1000 cm^{-1} , so it is difficult to detect them by FT-IR spectroscopy, owing to the strong IR absorption of the $\gamma-Al_2O_3$ supports in this region (see the Supporting Information, Figure S2).^[13,27] The XRD pattern of the $P_2W_{15}-Al_2O_3$ composite is similar to that of Al_2O_3 , indicating no diffraction of the $Na_{12}[\alpha-P_2W_{15}O_{56}] \cdot 24H_2O$ due to poor crystallinity and coexistence of other crystalline phases (see the Supporting Information, Figure S3). From the Raman spectra of $P_2W_{15}-Al_2O_3$ (Figure 2a), it can be seen that the $\gamma-Al_2O_3$ sup-

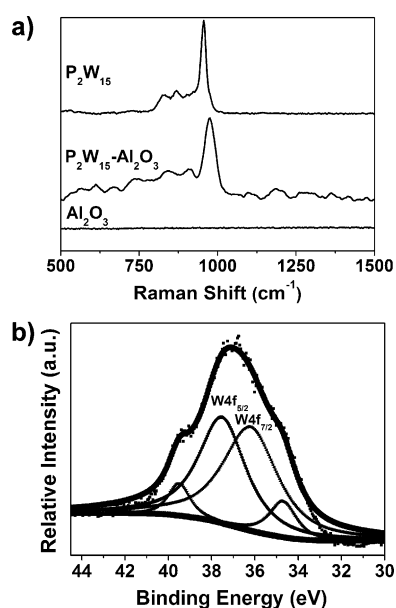


Figure 2. a) Raman spectra of Al_2O_3 , $P_2W_{15}-Al_2O_3$ and P_2W_{15} ; b) W4f X-ray photoelectron spectrum of $P_2W_{15}-Al_2O_3$.

port is not Raman active, allowing detection of all $W-O$ vibrations.^[28] The characteristic vibrations of bulk $\{P_2W_{15}\}$ are located at 955 , 871 , and 827 cm^{-1} , whereas $P_2W_{15}-Al_2O_3$ gives rise to Raman bands at 980 , 909 and 839 cm^{-1} , which can be assigned to the $W=O$ stretch bands and $W-O-W$ stretching modes of the immobilized cluster.^[29] The Raman shifts are due to the strong interactions between the trilacunary POM cluster and the $\gamma-Al_2O_3$ support, leading to a decrease in the cluster's and/or the alumina's local symmetry.^[30]

Additionally, X-ray photoelectron spectroscopy (XPS) was used to determine the oxidation states of metal centers. More specifically, the XPS spectrum for W4f (Figure 2b) revealed two peaks at 34.8 and 36.2 eV ,^[31,32] in the energy region of $W4f_{7/2}$, and two peaks at 37.5 , 39.5 eV ,^[33,34] in the energy region of $W4f_{5/2}$, which are consistent with a W^{VI} oxidation state. Thermogravimetric analysis of the $P_2W_{15}-Al_2O_3$ compo-

site (see the Supporting Information, Figure S4) under nitrogen in the temperature range of 25 to 800 °C revealed two main weight losses. The first loss of 1.9% in a temperature range of 25–207 °C can be attributed to the loss of the absorbed water and crystallization water molecules of the sample. The second weight loss of 1.4%, between 207 and 523 °C, can be assigned to the loss of the constitutional water from $P_2W_{15}-Al_2O_3$.^[35]

SEM images of the $P_2W_{15}-Al_2O_3$ composite material show sheet-like morphologies that are similar to that of the bare Al_2O_3 support (see the Supporting Information, Figures S5 and S6). The HR-TEM images of the $P_2W_{15}-Al_2O_3$ composite material revealed unambiguously the presence of $\{P_2W_{15}\}$ clusters on the $\gamma-Al_2O_3$ support, in the form of dark dots 1–2 nm in size (Figure 3). To further investigate the nature of the linkage be-

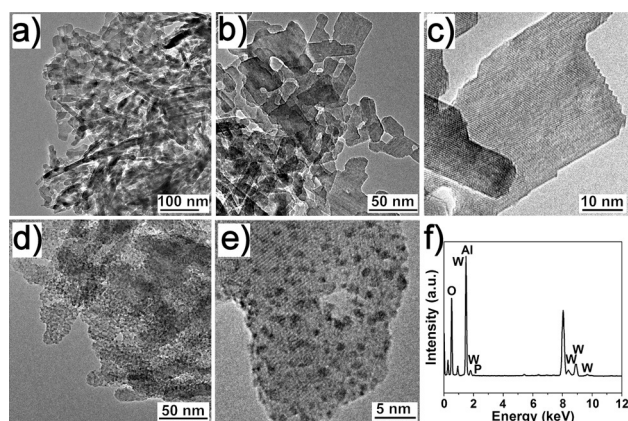


Figure 3. a–e) HR-TEM images of Al_2O_3 (a–c) and $P_2W_{15}-Al_2O_3$ (d,e); f) energy dispersive spectrum of $P_2W_{15}-Al_2O_3$.

tween the $\{P_2W_{15}\}$ clusters and the $\gamma-Al_2O_3$ support, we studied the stability of the $P_2W_{15}-Al_2O_3$ composite in LiCl solution, according to a previously reported procedure.^[13] The $P_2W_{15}-Al_2O_3$ composite materials were dispersed in 0.3 M LiCl solution under vigorous stirring for 12 h, removed by filtration, and dried under vacuum. The procedure was repeated three times; close examination of the HR-TEM images obtained from the collected and dried material (see the Supporting Information, Figure S7) showed that the POM clusters remained immobilized on the surface of $\gamma-Al_2O_3$ and inductively coupled plasma (ICP) analysis of the collected filtrates showed that no elemental W was present. The experimental data strongly suggest that the $\{P_2W_{15}\}$ clusters are not just physically adsorbed on the $\gamma-Al_2O_3$, since the presence of Li^+ counterions would have removed the clusters from the surface and extracted them into the solution. Examination of the elemental composition of the material by energy-dispersive spectroscopy (EDS) showed that P and W atoms are present on the $P_2W_{15}-Al_2O_3$ composite material (Figure 3 f) whereas X-ray fluorescence spectroscopy revealed that the loading of $\{P_2W_{15}\}$ on the $\gamma-Al_2O_3$ support was approximately 9.98%.

N_2 adsorption–desorption isotherms of $\gamma-Al_2O_3$ and $P_2W_{15}-Al_2O_3$ (Figure 4 and Table S1 in the Supporting Information) are classified as type IV with a clear H1-type hysteresis loop according to the IUPAC classification, indicating mesoporosity.

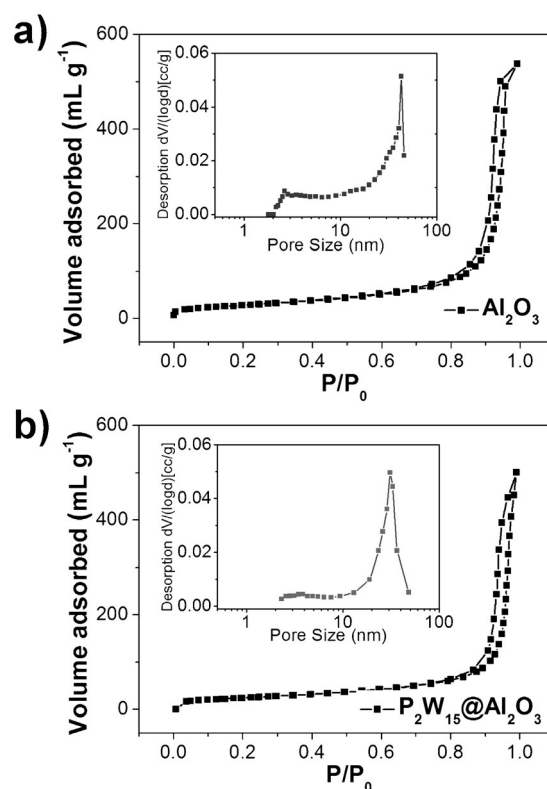
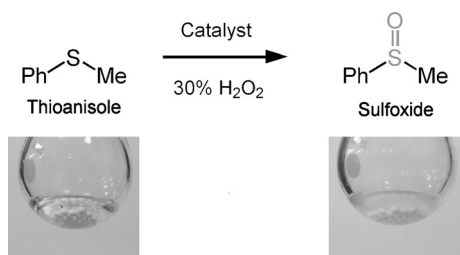


Figure 4. The N_2 adsorption–desorption isotherm and pore size distributions of Al_2O_3 (a) and $P_2W_{15}-Al_2O_3$ (b).

The pore size distribution curves of $\gamma-Al_2O_3$ and $P_2W_{15}-Al_2O_3$ showed mean pore sizes of 42.74 and 30.93 nm, respectively, indicating that the regular mesoporous channels of the $\gamma-Al_2O_3$ support are retained in the corresponding $P_2W_{15}-Al_2O_3$ catalysts. The pore sizes of $P_2W_{15}-Al_2O_3$ decreased with increased P_2W_{15} loading, which can be explained by the fact that the pores are partially blocked by $\{P_2W_{15}\}$ clusters.

Catalytic oxidation of organic compounds under mild conditions are of both considerable intellectual interest and potential utility.^[36,37] Catalytic oxidation of organic sulfides remains a topical interest due to the versatile utility of both sulfoxides and sulfones in organic synthesis.^[38–40] Although a multitude of oxygen donors are available, utilization of H_2O_2 as a “green” oxygen donor has become increasingly prominent.^[41–44] In this work, catalytic oxidation of thioanisole in the presence of $P_2W_{15}-Al_2O_3$ as catalyst and H_2O_2 as oxidant was carried out (Scheme 2). The selectivity of sulfoxide products and the conversion of the initial sulfides were quantified by using gas chromatography (GC; see the Supporting Information, Figures S8 and S9) and 1H NMR spectroscopy of the reactant (thioanisole) and the product upon completion of the reaction (Figure 5). Reactivity data for the oxidation of thioanisole in CH_3OH at 25 °C in the presence of the $\{P_2W_{15}\}$ and $P_2W_{15}-Al_2O_3$ and in the absence of the $P_2W_{15}-Al_2O_3$ are summarized in Table S2 (see the Supporting Information). In the presence of the $P_2W_{15}-Al_2O_3$ catalyst, conversion and selectivity were improved considerably. This indicates that the $P_2W_{15}-Al_2O_3$ is an effective catalyst for the oxygenation of thioanisole by H_2O_2 . To



Scheme 2. Selective oxidation of sulfides to sulfoxides by using the $P_2W_{15}-Al_2O_3$ composite as catalyst.

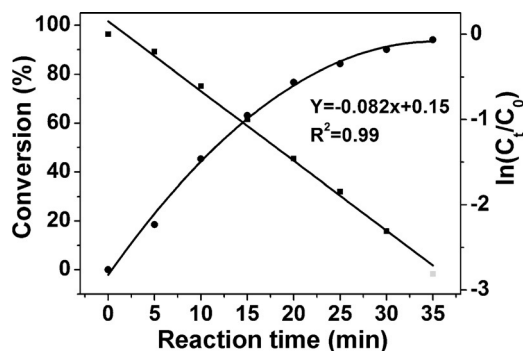


Figure 5. 1H NMR ($CDCl_3$) spectra of the reactant (thioanisole) and the product (sulfoxide). Experimental conditions: Thioanisole (1 mmol), H_2O_2 (1 mmol), catalyst (2.5 μ mol), CH_3OH (200 μ L), 25 $^\circ C$, 35 min.

optimize the reaction conditions, various solvents, reaction times, and amounts of H_2O_2 and catalyst were investigated (see the Supporting Information, Figures S10–S12 and Table S3). The determined optimal conditions were found to be the following: thioanisole (1 mmol), H_2O_2 (82 μ L), CH_3OH (200 μ L). Experiments to determine the kinetic parameters for the catalytic oxidation of thioanisole were carried out under these conditions.

Reaction kinetics for the oxidation of thioanisole are presented in Figure 6, where the (C_t/C_0) is plotted against the reaction time. C_0 and C_t are the initial thioanisole concentration and the

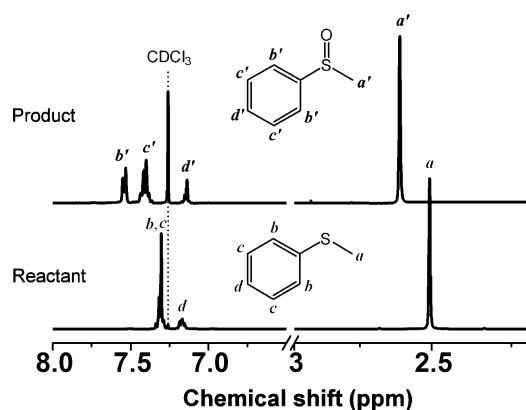


Figure 6. Catalytic conversion of thioanisole and $\ln(C_t/C_0)$ as functions of reaction time. Reaction conditions: Thioanisole (1 mmol), H_2O_2 (1 mmol), CH_3OH (200 μ L), 25 $^\circ C$, 35 min.

thioanisole concentration at time t , respectively. By using Equations (3) and (4), the rate constant k of the oxidation reaction was determined to be -0.082 min^{-1} . The oxidation of thioanisole and subsequent conversion to the product (sulfoxide) can be completed in about 35 min.

$$-\frac{dC_t}{dt} = kC_t \quad (3)$$

$$\ln \frac{C_0}{C_t} = kt \quad (4)$$

As such, the catalyst shows high catalytic efficiency for the oxidation of sulfides to sulfoxides, and the catalytic reaction exhibits pseudo-first-order kinetics for the oxidation of thioanisole with 99% selectivity for sulfoxides ($R^2 = 0.99$). In an effort to confirm that the catalyst is truly heterogeneous, we removed the catalyst from the reaction mixture when the conversion reached a value of 60% after 15 min. Real time monitoring of the reaction mixture by GC showed that the substrate catalytic conversion stopped immediately. The addition of the catalyst back to the reaction mixture restarted the reaction (see the Supporting Information, Figure S13).

After confirming the stability and efficiency of the composite material, we investigated the general applicability and selectivity of the as-prepared catalyst of $P_2W_{15}-Al_2O_3$. We utilized a series of thioether-based compounds as substrates in catalytic oxygenation reactions under the same conditions (Table 1). Alkyl aryl thioethers and 4-pentamethylene sulfides could be selectively fully converted into the desired product. However, 2-bromothioanisole underwent relatively low conversion, which might be due to increased steric hindrance and/or electrophilic effects (Table 1, entry 4). Interestingly, the phenyl allyl

Table 1. Oxidation of various sulfides to the corresponding sulfoxides.^[a]

Entry	Substrate	Product	Conv. [%] ^[b]	Sel. [%] ^[c]
1			94	99
2			90	99
3			98	97
4			34	100
5			94	97
6			63	92
7			96	91

[a] Experimental conditions: Substrate (1 mmol), 30% H_2O_2 (1 mmol), $P_2W_{15}-Al_2O_3$ (2.5 μ mol), CH_3OH (200 μ L), 25 $^\circ C$, 35 min; [b] conversion of sulfides; [c] selectivity towards sulfoxides.

thioether underwent 63% conversion into the desired sulfoxide alongside an unknown byproduct (Table 1, entry 6).

The main advantage of using a heterogeneous catalysts in a liquid-phase reaction is the ease of separation and recycling of the catalyst. To test whether any catalyst leaching occurred, we filtered off the catalyst after each cycle, washed it with acetone, dried and then added it into a fresh reaction mixture. The solid-state ^{31}P NMR (Figure 7a) and Raman spectra (Figure 7b) and the HR-TEM image (Figure 7c) of the recovered

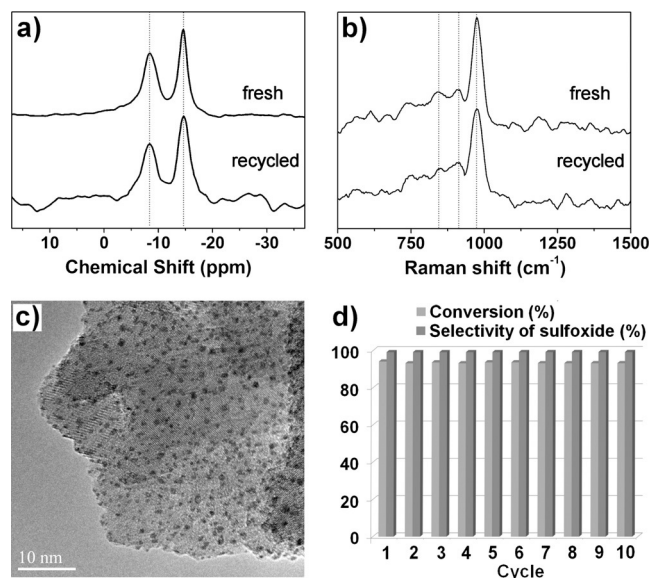


Figure 7. a) Solid state ^{31}P NMR spectra and b) Raman spectra of the fresh and recycled $\text{P}_2\text{W}_{15}\text{-Al}_2\text{O}_3$ after 10 cycles; c) HR-TEM image of the recycled catalyst after 10 cycles; d) recycling experiments for selective oxidation of sulfides to sulfoxides catalyzed by $\text{P}_2\text{W}_{15}\text{-Al}_2\text{O}_3$. Experimental conditions: Thioanisole (1 mmol), H_2O_2 (1 mmol), catalyst (2.5 μmol), CH_3OH (200 μL), 25 $^\circ\text{C}$, 35 min.

catalyst after 10 cycles were almost the same as those of the fresh one, indicating the stability of the catalyst. The aged $\text{P}_2\text{W}_{15}\text{-Al}_2\text{O}_3$ catalytic system can be reused for the oxidation of thioanisole, promoting the oxidation of sulfides to sulfoxides, at least ten times without significant decrease of its catalytic efficiency (Figure 7d). The catalytic efficiencies of various previously reported systems for the oxidation of sulfide substrates are summarized in Table S4 (see the Supporting Information). The high efficiency and selectivity of the $\text{P}_2\text{W}_{15}\text{-Al}_2\text{O}_3$ catalyst, along with its quick and easy preparation in a single step and lower consumption of H_2O_2 during the catalytic conversion of the substrates (Table S4, entry 14), render it an ideal candidate for larger scale application.

Conclusion

The immobilization of P_2W_{15} clusters on spherical $\gamma\text{-Al}_2\text{O}_3$ particles results in the formation of $\text{P}_2\text{W}_{15}\text{-Al}_2\text{O}_3$ as a new heterogeneous catalyst, in which strong covalent bonds are formed between the $[\alpha\text{-P}_2\text{W}_{15}\text{O}_{56}]^{12-}$ clusters and the hydroxyl groups of the spherical $\gamma\text{-Al}_2\text{O}_3$ support inducing exceptional stability to

the catalytic system. Moreover, the P_2W_{15} clusters are distributed uniformly onto the $\gamma\text{-Al}_2\text{O}_3$ surface as evidenced by HR-TEM studies. Highly efficient and selective oxygenation of thioethers can be achieved by the $\text{P}_2\text{W}_{15}\text{-Al}_2\text{O}_3$ in the presence of H_2O_2 with 99% selectivity of sulfoxides and 94% conversion in 35 min. The $\text{P}_2\text{W}_{15}\text{-Al}_2\text{O}_3$ can be separated easily by filtration and reused at least ten times without obvious decrease in catalytic efficiency. The facile preparation, reusability, and efficacy of the heterogeneous $\text{P}_2\text{W}_{15}\text{-Al}_2\text{O}_3$ catalyst provide great potential for industrial applications. Finally, the straightforward covalent attachment of the appropriate choice of the polyoxometalate core (architecture and composition) opens the door for further exploration and design of multifunctional catalytic materials tailored for specific applications. Our current research effort is focused on exploring the potential of the family of $\text{POM-Al}_2\text{O}_3$ catalysts for the development of chiral sulfoxides.

Experimental Section

Chemicals and Materials

All chemicals were of analytical grade and were used as received without any further purification. Thioether compounds were purchased from Alfa Aesar. LiCl , HCl , KNO_3 , HNO_3 , and NaOH were purchased from Beijing Chemical Reagent Company (Beijing, China). Acetone, methanol, ethanol, acetonitrile, and ethyl acetate were purchased from J&K Chemical Ltd. Spherical $\gamma\text{-Al}_2\text{O}_3$ was purchased from Shandong Bente Chemical Corporation. Deionized water from a Millipore water purification system was used throughout the experiments. $\text{Na}_2[\alpha\text{-P}_2\text{W}_{15}\text{O}_{56}]\cdot 24\text{H}_2\text{O}$ (P_2W_{15}) was prepared according to a reported procedure.^[25]

Instruments

Solid-state NMR experiments were carried out at 10 kHz for ^{31}P on a Bruker Avance 300 MHz solid-state spectrometer equipped with a commercial 5 mm MAS NMR probe. FT-IR spectra were collected in transmission mode by using a JASCO FT-IR 410 spectrometer or a JASCO FT-IR 4100 spectrometer (wavenumbers ν are given in cm^{-1} ; intensities are denoted as wk=weak, sh=sharp, m=medium, br=broad, s=strong). XRD measurements were performed on a JCN Ultima III X-ray diffractometer. XPS data were obtained from a Thermo-Fisher Scientific ESCALAB 250 X-ray photoelectron spectrometer. TGA measurements were performed on a DTG-60 A analyzer from the Shimadzu Corporation, under nitrogen atmosphere with a temperature increase of 10 $^\circ\text{C min}^{-1}$ between 25 and 800 $^\circ\text{C}$. Laser Raman spectra were obtained by using a LabRAM ARAMIS Raman spectrometer. Scanning emission microscope (SEM) images were collected on a Zeiss Supra 55 VP field-emission scanning electron microscope. High-resolution transmission electron microscopy (HR-TEM) images were obtained with a JEOL JEM-3010 microscope operated at 300 kV. BET data were obtained by using a Bei Shi De 3H-2000PS2 specific surface area and pore size analyzer. X-Ray fluorescence spectra were obtained by using a XRF-1800 with a scanning rate of 20 $^\circ \text{min}^{-1}$. The content of sulfides and sulfoxides were analyzed on an Agilent 7820 A GC system using a 30 m 5% phenylmethyl silicone capillary column with an ID of 0.32 mm and 0.25 mm coating (HP-5).

Synthesis of P₂W₁₅–Al₂O₃

Spherical γ -Al₂O₃ was activated at 900 °C under atmospheric pressure for 24 h, then cooled to room temperature in accordance with the procedure reported by Cargnello et al.^[45] In a reaction vessel, Na₁₂[(α -P₂W₁₅O₅₆)]·24H₂O (1.66 × 10⁻⁴ mol) was dissolved as a clear solution in deionized water (50 mL) without CO₂, and then γ -Al₂O₃ spheres (1 g) were added to the solution. The pH of the solution was adjusted to 1.00 carefully by dropwise addition of 4 M aqueous HCl. The reaction mixture was stirred at room temperature for 1 h and then at 90 °C for 3 h.^[46] The reaction mixture was cooled to room temperature and the product was removed by filtration, washed with 0.3 M LiCl solution (3 × 100 mL), and dried under vacuum at 60 °C for 24 h.

Determination of isoelectric points

The isoelectric point (IEP) of the γ -Al₂O₃ support was determined by a batch equilibration method, as described in the literature.^[47] The spherical γ -Al₂O₃ support (25 mg) was dispersed in 0.1 M aqueous KNO₃ (25 mL) with vigorous stirring for 60 min. Six bottles of the resultant solution were prepared and the pH values of the bottles were adjusted to 3, 4, 5, 6, 7, 8, 9, 10, and 11 by addition of aqueous HNO₃ (0.1 M) or NaOH (0.1 M). The zeta potential of each solution was measured and plotted as a function of pH (see the Supporting Information, Figure S1). The pI_{IEP} value (ca. 8.6) of the γ -Al₂O₃ support was determined at the point of zeta potential = 0.

Catalytic test

The oxidation reaction was carried out in a 25 mL flask with magnetic stirring. A typical optimized procedure was as follows: Thioanisole (1 mmol), H₂O₂ (1 mmol), CH₃OH (200 μ L), P₂W₁₅–Al₂O₃ (2.5 μ mol; 9.98% loading of P₂W₁₅ on Al₂O₃) were added to the flask. The reaction time was counted after addition of the catalyst (T = 25 °C). Before GC measurement, the reaction mixture was quenched by adding the deionized H₂O (1 mL) and diethyl ether (6 mL). After stirring for 1 min, it was filtered through a 0.22 μ m microfilter, and the filtrate was analyzed by GC. The yield was determined by using reference standards. No increase of conversion can be found after 35 mins. After completion of the reaction, the catalyst was recovered by filtration, washed with the acetone (20 mL), and dried in the oven at 60 °C.

Acknowledgements

This research was supported by the National Basic Research Program of China (973 program, 2014CB932104), the National Science Foundation of China (U1407127, U1507102), and Fundamental Research Funds for the Central Universities (RC1302, YS1406). W.C. appreciates financial support from the China Postdoctoral Science Foundation (2014M560878).

Keywords: alumina · immobilization · oxidation · polyoxometalates · supported catalysts

- [1] a) H. N. Miras, J. Yan, D. L. Long, L. Cronin, *Chem. Soc. Rev.* **2012**, *41*, 7403–7430; b) S. Herrmann, M. Kostrzewa, A. Wierschem, C. Streb, *Angew. Chem. Int. Ed.* **2014**, *53*, 13596–13599; *Angew. Chem.* **2014**, *126*, 13814–13817.
[2] M. T. Pope in *NATO Science Series, Vol. 98: Polyoxometalate Molecular Science* (Eds.: J. J. Borrás-Almenar, E. Coronado, A. Müller, M. T. Pope), Springer, Heidelberg, **2003**, pp. 3–31.

- [3] S. Omwoma, W. Chen, R. Tsunashima, Y. F. Song, *Coord. Chem. Rev.* **2014**, *258–259*, 58–71.
[4] V. Rives, D. Carriazo, C. Martin in *Pillared Clays and Related Catalysts* (Eds.: A. Gil, S. A. Korili, R. Trujillo, M. A. Vicente), Springer, Heidelberg, **2010**, pp. 319–422.
[5] F. Bentaleb, O. Makrygenni, D. Brouri, C. C. Diogo, A. Mehdi, A. Proust, F. Launay, R. Villanneau, *Inorg. Chem.* **2015**, *54*, 7607–7616.
[6] L. Liu, B. Wang, Y. Du, A. Borgna, *Appl. Catal. A* **2015**, *489*, 32–41.
[7] G. S. Armatas, G. Bilis, M. Louloudi, *J. Mater. Chem.* **2011**, *21*, 2997–3005.
[8] L. Marleny Rodriguez-Albelo, A. R. Ruiz-Salvador, A. Sampieri, D. W. Lewis, A. Gómez, B. Nohra, P. Mialane, J. Marrot, F. Sécherresse, C. M. Draznieks, R. N. Biboum, B. Keita, L. Nadjo, A. Dolbecq, *J. Am. Chem. Soc.* **2009**, *131*, 16078–16087.
[9] J. Suárez-Guevara, V. Ruiz, P. Gomez-Romero, *J. Mater. Chem. A* **2014**, *2*, 1014–1021.
[10] B. Li, W. Ma, J. Liu, S. Zuo, X. Li, *J. Colloid Interface Sci.* **2011**, *362*, 42–49.
[11] J. C. Juan, J. Zhang, M. A. Yarmo, *J. Mol. Catal. A* **2007**, *267*, 265–271.
[12] Z. Zhang, F. Zhang, Q. Zhu, W. Zhao, B. Ma, Y. Ding, *J. Colloid Interface Sci.* **2011**, *360*, 189–194.
[13] G. S. Armatas, A. P. Katsoulidis, D. E. Petrakis, P. J. Pomonis, *J. Mater. Chem.* **2010**, *20*, 8631–8638.
[14] L. Zhou, L. Wang, S. Zhang, R. Yan, Y. Diao, *J. Catal.* **2015**, *329*, 431–440.
[15] H. S. Potdar, K. W. Jun, J. W. Bae, S. M. Kim, Y. J. Lee, *Appl. Catal. A* **2007**, *321*, 109–116.
[16] H. C. Lee, H. J. Kim, C. H. Rhee, K. H. Lee, J. S. Lee, S. H. Chung, *Microporous Mesoporous Mater.* **2005**, *79*, 61–68.
[17] X. Zhang, F. Zhang, K. Y. Chan, *Mater. Lett.* **2004**, *58*, 2872–2877.
[18] O. Mekasuwandumrong, V. Pavarajarn, M. Inoue, P. Praserttham, *Mater. Chem. Phys.* **2006**, *100*, 445–450.
[19] B. Xua, T. Xiao, Z. Yan, X. Sun, J. Sloan, S. L. González-Cortés, F. Alshahrani, M. L. H. Greena, *Microporous Mesoporous Mater.* **2006**, *91*, 293–295.
[20] J. Aguado, J. Escola, M. Castro, B. Paredes, *Microporous Mesoporous Mater.* **2005**, *83*, 181–192.
[21] H. Farag, D. Whitehurst, K. Sakanishi, I. Mochida, *Catal. Today* **1999**, *50*, 9–17.
[22] R. Maggi, R. Ballini, G. Sartori, R. Sartorio, *Tetrahedron Lett.* **2004**, *45*, 2297–2299.
[23] F. M. Mulcahy, M. J. Fay, A. Proctor, M. Houalla, D. M. Hercules, *J. Catal.* **1990**, *124*, 231–240.
[24] N. K. Nag, *J. Phys. Chem.* **1987**, *91*, 2324–2327.
[25] R. Contant, W. G. Klemperer, O. Yaghi, *Inorg. Synth.* **1990**, *27*, 104–111.
[26] N. V. Izarova, R. I. Maksimovskaya, S. Willbold, P. Kögerler, *Inorg. Chem.* **2014**, *53*, 11778–11784.
[27] I. E. Wachs, *Catal. Today* **1996**, *27*, 437–455.
[28] E. I. Ross-Medgaarden, I. E. Wachs, *J. Phys. Chem. C* **2007**, *111*, 15089–15099.
[29] W. Tao, Z. Li, D. Pan, L. Nie, S. Yao, *J. Phys. Chem. B* **2005**, *109*, 2666–2672.
[30] C. Feng, H. Shang, X. Liu, *Chin. J. Catal.* **2014**, *35*, 168–174.
[31] W. Grünert, R. Feldhaus, K. Anders, E. S. Shpiro, G. V. Antoshin, Kh. M. Minachev, *J. Electron Spectrosc. Relat. Phenom.* **1986**, *40*, 187–192.
[32] P. Biloen, G. Pott, *J. Catal.* **1973**, *30*, 169–174.
[33] B. V. R. Chowdari, K. L. Tan, W. T. Chia, *Solid State Ionics* **1992**, *53*, 1172–1178.
[34] G. P. Halada, C. R. Clayton, *J. Vac. Sci. Technol. A* **1993**, *11*, 2342–2347.
[35] Y. Guo, Y. Wang, C. Hu, Y. Wang, E. Wang, *Chem. Mater.* **2000**, *12*, 3501–3508.
[36] K. A. Joergensen, *Chem. Rev.* **1989**, *89*, 431–458.
[37] B. Meunier, *Chem. Rev.* **1992**, *92*, 1411–1413.
[38] I. Fernández, N. Khair, *Chem. Rev.* **2003**, *103*, 3651–3706.
[39] M. Mikolajczyk, J. Drabowicz, P. Kielbasinski, *Chiral Sulfur Reagents: Applications in Asymmetric and Stereoselective Synthesis*, CRC Press, Boca Raton, FL, **1997**.
[40] T. D. Phan, M. A. Kinch, J. E. Barker, T. Ren, *Tetrahedron Lett.* **2005**, *46*, 397–400.
[41] N. M. Gresley, W. P. Griffith, A. C. Laemmel, H. I. Nogueira, B. C. Parkin, *J. Mol. Catal. A* **1997**, *117*, 185–198.

- [42] M. Carraro, N. Nsouli, H. Oelrich, A. Sartorel, A. Sorarù, S. S. Mal, G. Scorrano, L. Walder, U. Kortz, M. Bonchio, *Chem. Eur. J.* **2011**, *17*, 8371–8378.
- [43] K. Kamata, T. Hirano, S. Kuzuya, N. Mizuno, *J. Am. Chem. Soc.* **2009**, *131*, 6997–7004.
- [44] J. M. Brégeault, M. Vennat, L. Salles, J. Y. Piquemal, Y. Mahha, E. Briota, P. C. Bakalaa, A. Atlamsanic, R. Thouvenotd, *J. Mol. Catal. A* **2006**, *250*, 177–189.
- [45] M. Cargnello, J. J. D. Jaén, J. C. H. Garrido, K. Bakhmutsky, T. Montini, J. J. C. Gámez, R. J. Gorte, P. Fornasiero, *Science* **2012**, *337*, 713–717.
- [46] C. N. Kato, T. Kashiwagi, W. Unno, M. Nakagawa, H. Uno, *Inorg. Chem.* **2014**, *53*, 4824–4832.
- [47] S. Vidojkovic, V. Rodriguez-Santiago, M. V. Fedkin, D. J. Wesolowski, S. N. Lvov, *Chem. Eng. Sci.* **2011**, *66*, 4029–4035.

Received: April 20, 2016

Published online on July 11, 2016